JACS
JOURNAL OF THE AMERICAN CHEMICAL SOCIETY
Article
pubs.acs.org/JACS

The Formation of Ti−H Species at Interface Is Lethal to the Efficiency of TiO_2-Based Dye-Sensitized Devices

Yan Yan,[†,‡] Weidong Shi,[‡] Zhen Yuan,[†] Shenggui He,[†] Dongmei Li,[§] Qingbo Meng,[§] Hongwei Ji,[†] Chuncheng Chen,[†] Wanhong Ma,*[,†] and Jincai Zhao*[,†]

[†]Key Laboratory of Photochemistry and State Key Laboratory for Structural Chemistry of Unstable and Stable Species, Beijing National Laboratory for Molecular Sciences, Institute of Chemistry, Chinese Academy of Sciences, Beijing, P. R. China 100190

[‡]School of Chemistry and Chemical Engineering, Jiangsu University, No. 301, Xuefu Road, Zhenjiang, P. R. China 212013

[§]Key Laboratory for Renewable Energy (CAS), Beijing Key Laboratory for New Energy Materials and Devices, Beijing National Laboratory for Condensed Matter Physics, Institute of Physics, Chinese Academy of Sciences, Beijing, P. R. China 100190

Supporting Information

ABSTRACT: TiO_2-based dye-sensitization cycle is one of the basic strategies for the development of solar energy applications. Although the power conversion efficiency (PCE) of dye-sensitized devices has been improved through constant attempts, the intrinsically fatal factor that leads to the complete failure of the PCE of TiO_2-mediated dye-sensitized devices has not yet been determined. Here, by using isotopically labeled MAS−^{1}H NMR, ATR-FTIR spectroscopy (separate H/D and ^{48}Ti/^{49}Ti experiments), and ESR, we revealed that the accumulative formation of Ti−H species on the TiO_2 surface is the intrinsic cause of the PCE failure of TiO_2-based dye-sensitization devices. Such a Ti−H species is generated from the reduction of hydrogen ions (mostly released from dye carboxyl groups or organic electrolyte) accompanied by electron injection on the surface of TiO_2, which deteriorates the PCE mainly by reducing the electrical conductivity of the TiO_2 (by a maximum of ∼80%) and the hydrophilic nature of the TiO_2 surface (contact angle increased).

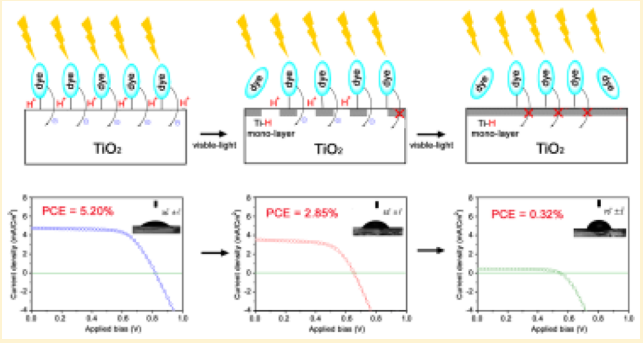

INTRODUCTION

Wide band gap oxide semiconductors such as TiO_2 (E_{gap} ≈ 3.2 eV) and ZnO (E_{gap} ≈ 3.4 eV) do not absorb visible light. However, dye-sensitization strategies, which originated from the sandwich-type dye-sensitized solar cells developed 25 years ago,[1] enable these semiconductors to utilize visible light in solar energy conversion applications such as dye-sensitized solar cells (DSSCs),[2,3] dye-sensitized photoelectrochemical water splitting,[4,5] sensing[6] and dye-sensitized photocatalysis for environmental remediation and selective organic synthesis.[7] Among popular oxide semiconductor materials, TiO_2 in either the film or powder form is the first choice because of its reasonable cost with respect to other semiconductors, the environmental compatibility and excellent capacity for stable operation with a turnover number (TON) of more than 10 000.[8−10] By employing the TiO_2 film as electron transport layer (ETL), Saliba et al. improved the solar energy conversion efficiency of inorganic/organic hybrid perovskite solar cells to a new record of ∼21.1%.[11]

In a typical dye-sensitization prototype, dye molecules are excited by visible light, and the excited electrons are subsequently injected, trapped, and transferred to the external circuit or different substrates at the liquid/dye-TiO_2 interface. Unlike the electron transfer (ET) inside the interior of bulk TiO_2, the interfacial electron injection and trapping on TiO_2 surface involve both the electrical redox states of TiO_2 and the chemical states on the surface. Especially, protons (mostly originated from the carboxyl and amino groups of the dyes) and potential proton donors (the oxidation of organic C−H groups) are almost inevitable in all dye-sensitized systems. Therefore, in the view of chemical reactions, an electrical redox relaxation of Ti^{4+}/Ti^{3+} coupled with proton transfer (PT) is always required to accomplish the electron injection, trapping and transfer at the liquid/dye-TiO_2 interface.[12−15] Such a reversible proton-coupled electron transfer (PCET) process on TiO_2 surface ($Ti^{4+}-O^- + H^+ + e^- \leftrightarrow Ti^{3+}-OH$) generally determines the whole PCE of TiO_2-based dye-sensitized devices by two aspects: (i) affects the electron transport ability at liquid/TiO_2 interface, and (ii) maintains the TiO_2 surface polarity for tightly anchoring dye molecules. For now, the dye-sensitized electron trapping and corresponding PT reaction on TiO_2 surface under visible light irradiation has long been considered identical to these in the UV direct excitation case,

Received: December 2, 2016
Published: January 15, 2017

DOI: 10.1021/jacs.6b12324
J. Am. Chem. Soc. 2017, 139, 2083−2089

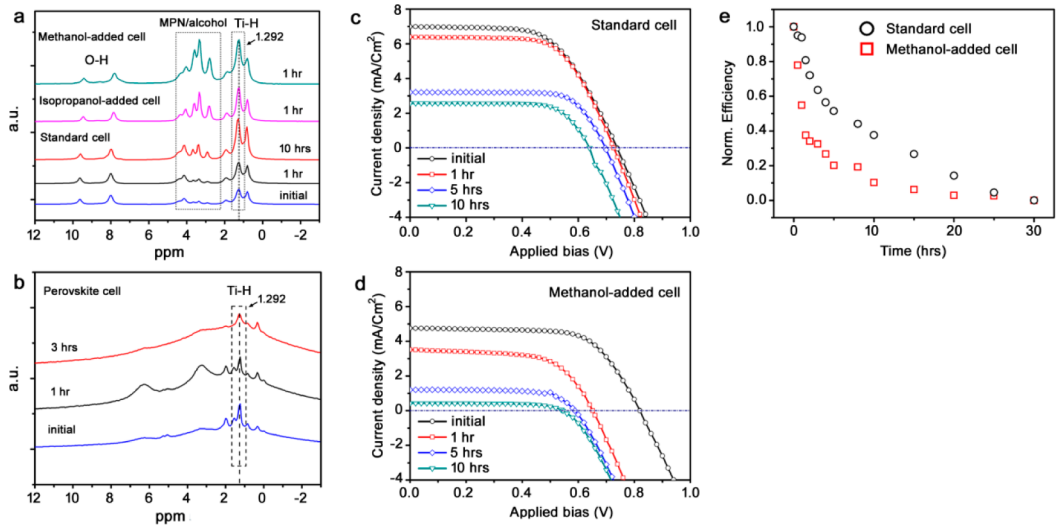

Figure 1. MAS NMR ^{1}H spectra and performance of N719-DSSCs and $CH_3NH_3PbI_3$ perovskite cells during continuous operation under simulated AM1.5 sunlight of 100 mW/cm^2 irradiation. For N719-DSSCs, different cells were distinguished by different electrolyte solvent compositions: pure 3-methoxypropionitrile (MPN) in standard cells; a methanol/MPN mixed solvent (v/v = 1:9) in methanol-added cells; and a isopropanol/MPN mixed solvent (v/v = 1:9) in isopropanol-added cells. Devices were encapsulated under an inert atmosphere. (a) MAS NMR ^{1}H spectra of TiO_2 samples scratched from photoanodes of different N719-DSSCs before and after continuous operation for certain times. (b) MAS NMR ^{1}H spectra of TiO_2 samples scratched from photoanodes of $CH_3NH_3PbI_3$ perovskite cells before and after continuous operation for certain times. (c, d) Current−voltage curves of standard and methanol-added cells, respectively, measured under simulated AM1.5 sunlight at 100 mW/cm^2 during various stages of operation; the curves show rapid deterioration of device performance. (e) Normalized solar cell PCE values during continuous operation (detailed solar cell PV metrics data are listed in Supplementary Table 1).

with only the difference of electron sources. Very recently, a few reports have observed the decrease in the PCE of TiO_2-mediated dye-sensitized systems when protons were intentionally added to the system.[16,17] Such a surface proton-induced efficiency drop clearly differs from the case of UV direct excitation of TiO_2 and contradicts the above traditional chemical transformation principle of TiO_2-mediated ET and PT.[15,18,19] More importantly, although the PCE failure of TiO_2-based dye-sensitized systems was often observed after long- or short-term operations,[20,21] the ET- and PT-induced TiO_2 surface transition has never been suspected as a liable perpetrator as others, such as the dye decomposition and electrolyte leakage. Here, we reveal a fundamental fact that for most dye-sensitized applications, in accompany with the reversible Ti^{4+}/Ti^{3+} redox relaxation circle, an irreversible Ti−H species is accumulatively generated on the TiO_2 surface under visible light irradiation, which directly deteriorates the conductivity and hydrophilic nature of TiO_2, and can cause the complete failure of PCE by covering TiO_2 surface without dye-decomposition and electrolyte leakage.

EXPERIMENTAL SECTION

Experimental instruments, chemicals, and detailed protocols are described in the Supporting Information.

MAS NMR ^{1}H Measurement. For DSSC samples, different cells were decapsulated, and the coated TiO_2 photoanode films were scraped off in Ar atmosphere. Products were then transferred into a zironia rotor (7 mm in diameter), and then the rotor was sealed for MAS NMR measurement. For TiO_2 powder samples, reduced TiO_2 methanol solution was dried by Argon flow at 50 °C. Dried products were then transferred into a zironia rotor (7 mm in diameter) in Ar glovebox, and then the rotor was sealed for MAS NMR measurement. The chemical shifts were calibrated by Deuterated water (D_2O) at 4.800 ppm.

ESR Measurement. Low temperature (90 K) ESR measurement was employed to observe Ti^{3+} signals of reduced TiO_2 sample after ex-situ UV-light and visible light irradiation, respectively. Before the measurement, reduced TiO_2 solutions with different irradiation times were collected and filled into a special cavity in the Argon glovebox and sealed. The obtained sample was then cooled to 90 K by liquid Nitrogen. The settings for the ESR spectrometer were as follows: center field, 3400 G; sweep width, 400/800 G; microwave frequency, 9.52 GHz; field modulation frequency, 100 kHz.

ATR-FTIR Measurement. ATR-FTIR measurement was employed to detect the surface species as well as their changes with in situ reaction process on TiO_2 films. The ATR-FTIR spectroscopy experimental setup was similar to that described in references.[31,32] The instrumental setup consisted of a Harrick Horizon multiple internal reflection accessories that were coupled to a 4 mL flow through cell containing a ZnSe crystal on the bottom plate and a quartz window on the top plate. Eleven infrared bounces were allowed using a 45° internal reflection element (50 × 10 × 2 mm^3). The FT-IR measurements were performed on a Nicolet 8700 FTIR with a DTGS detector. In a typical dye-sensitized procedure, a layer of 10^{-5} M dye (RhB, N3 or N719) methanol-d_0/d_4 solution was dripped onto the surface of the ZnSe crystal that was coated with a TiO_2 (^{49}Ti-labeled and unlabeled) film. The apparatus was degassed by Argon for 30 min and the crystal was then scanned to obtain the background spectrum. Time-resolved in situ FTIR data was then collected at the same time turning up the 550 nm LED lamp (3 W). The UV-excited case was similar to the dye-sensitized case except the absence of dyes and the employed LED lamp was switched to 365 nm (3W). FTIR data of TiH_2/TiD_2 was collected by dipping the acetonitrile solution of TiH_2/TiD_2 on the TiO_2 film and then dried by Argon flow. The TiD_2 sample was synthesized by the reaction of metal Ti powders and D_2 gas (XRD see Supplementary Figure 5c). In a typical synthetic procedure, 100 mg of Ti powder was heated at 500 °C in 5% D_2/Ar mixed atmosphere for 4 h, then cooled to room temperature.

Surface Contact Angle Measurement. Measurements were conducted on OCA20 mechine (Data-Physics, Germany). A single droplet volume for each measurement was 2 uL. The used TiO_2 sample was impact coated on FTO substrate (3 cm × 2.5 cm) by hydrothermal method according to reference.[30] Before measurements, corresponding substrates were immersed in methanol (with 10^{-5} M RhB in dye-sensitized case) and irradiated by UV and visible light

DOI: 10.1021/jacs.6b12324
J. Am. Chem. Soc. 2017, 139, 2083−2089

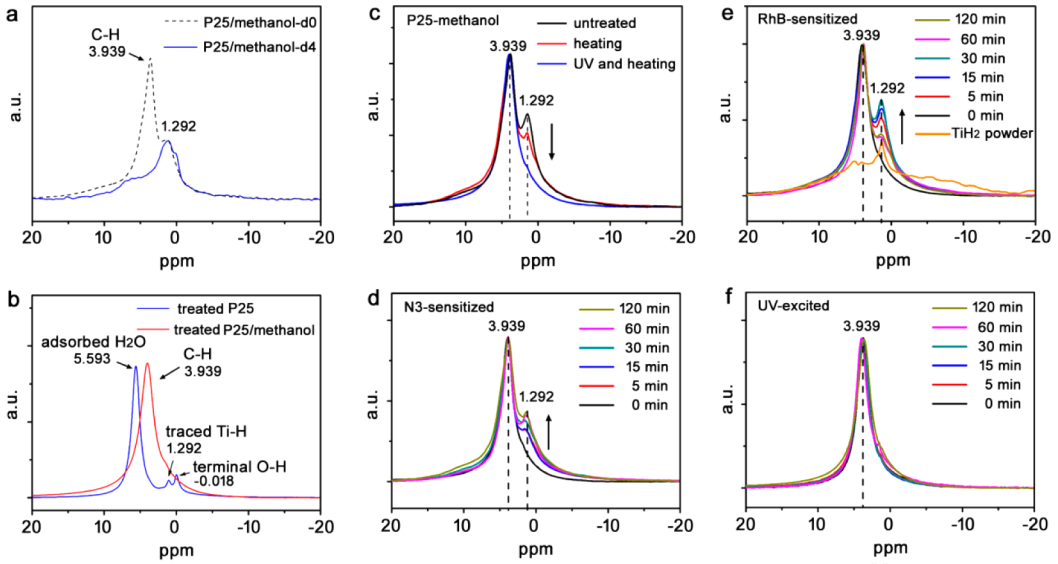

Figure 2. MAS NMR ^{1}H spectra of different TiO_2 samples before and after dye-sensitized operations. All solid samples were separated, dried, and prepared under an argon atmosphere (glovebox) prior to MAS NMR measurements. (a) MAS NMR ^{1}H spectra of P25 TiO_2 samples dried from methanol-d_0/-d_4 used to identify the missing C−H signals at 3.939 ppm from methanol. (b) MAS NMR ^{1}H spectra of pretreated P25 TiO_2 and pretreated P25 TiO_2 methanol-loaded samples. (c) MAS NMR ^{1}H spectra of different methanol-loaded P25 TiO_2 solid samples. Prior to methanol loading, P25 TiO_2 samples were pretreated using different methods (heating and UV irradiation in water) to eliminate the hydrogen species responsible for the peak at 1.292 ppm. (d) MAS NMR ^{1}H spectra of surface-treated P25 TiO_2 samples after visible-light irradiation (420 nm cutoff) in 10^{-5} M N3 dye methanol solution for different time periods (0−120 min). (e) MAS NMR ^{1}H spectra of surface-treated P25 TiO_2 solid samples after visible-light irradiation (420 nm cutoff) in 10^{-5} M RhB methanol solution for different time periods (0−120 min) and compared with the pristine TiH_2 solid powder (orange) as the control. (f) UV-irradiated (without filter) samples under identical conditions, except without the dyes.

respectively for different times (0−12 h), and then kept in argon atmosphere.

IC Analysis. The concentration of I^- ion was measured using a DX-900 Ion Chromatograph with an IonPac AS23 column (Dionex). The eluent for the IC was an 30 mM KOH solution, the curb was 20 mA, and the flow rate was 0.7 mL/min. The identification of I^- ions by IC analysis was performed using an observed retention time of approximately 15.3 min.

HPLC Analysis. The concentration of benzoic acid was analyzed using a Shimadzu HPLC system (LC-20AT pump and UV−vis SPD-20A detector) with a Dikma Diamond C-18 column (250 × 4.6 mm^2, 5 μm film thickness). The mobile phase was 25% acetonitrile in 75% water (1% formic acid solution) at 0.2 mL/min, and the detector wavelength was set at 254 nm. Quantification was performed using a calibration curve of benzoic acid.

RESULTS AND DISCUSSION

The Formation of Ti−H Surface Species and PCE Failure in Both TiO_2-Based DSSCs and TiO_2 Suspension Systems. First, we used solid-state magic angle spinning nuclear magnetic resonance (MAS ^{1}H NMR) spectroscopy to monitor specific proton-containing species on TiO_2 photoanodes in both general N719-DSSCs and alcohol-added DSSCs under standard AM1.5 sun irradiation (100 mW cm^{-2}). All DSSC devices were prepared under identical conditions, e.g., pre-encapsulated under an inert atmosphere, to eliminate the influence of electrolyte leakage, oxidation, moisture, or other effects. Simultaneously, two types of DSSCs (i.e., a standard set and an alcohol-added set) were prepared using the otherwise identical compositions and assembly conditions, with a small amount of methanol or isopropanol initially added to the 3-methoxypropionitrile (MPN) electrolyte in one of the sets (v/v = 1:9) used as control groups to provide extra proton sources for comparison. After different irradiation times, the cells were decapsulated, and the coated TiO_2 photoanode films were scraped off for ^{1}H MAS NMR characterization (Figure 1a). Prior to and following operations of the cell under AM 1.5 sun irradiation, a peak at 1.292 ppm was clearly and constantly observed and increased significantly with increasing irradiation time relative to the peaks of the terminal and bridging O−H signals at 0.8 ppm and 8−9.7 ppm,[22,23] respectively. The signals of the organic electrolyte solvent (MPN/alcohol) were observed at 2.5−4.3 ppm (Figure 1a bottom). For alcohol-containing control groups, nearly all observed peak positions were identical to those of the normal cells; however, the intensity of the peak at 1.292 ppm was obviously enhanced compared to that of the normal cells (Figure 1a top). This 1.292-ppm peak can also always be observed during the continuous irradiation of the standard TiO_2-based $CH_3NH_3PbI_3$ perovskite solar cells (Figure 1b). Moreover, we evaluated the performance of the DSSCs during continuous operation and observed simultaneous deterioration of the J_{sc} and PCE values (Figure 1c−e) with the increase in the peak at 1.292 ppm. In particular, J_{sc} always decreased faster in the cell with the added methanol than in the normal cells (Figure 1c, e). According to the conventional view, cell deactivation should be arised from the destruction of dyes or the electrolyte solution leakage. However, for a failed cell after 30 h of operation (PCE nearly complete lose), neither massive inactivation of the dyes nor electrolyte leakage was observed (Supplementary Figure 1), with the exception that the TiO_2 layer was covered by a new H-containing species with ^{1}H NMR peak at 1.292 ppm. This PCE failure without massive dye-decomposition is reminiscent of our previous work on H_2 evolution from Alizarin Red (AR)-sensitized Pt-TiO_2 aqueous suspending system driven by visible-light,[8] in which the sensitizing reaction was completely stopped after 80 h of operation (PCE completely lost); however, with ∼61% of the AR dye was still intact in the system at the moment. Both cases

DOI: 10.1021/jacs.6b12324
J. Am. Chem. Soc. 2017, 139, 2083−2089

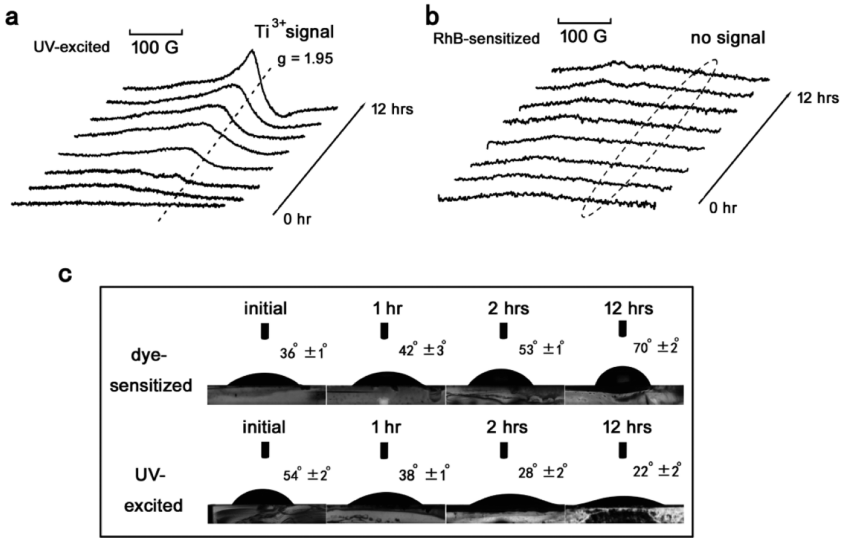

Figure 3. Ex situ low-temperature (90 K) ESR spectra of TiO_2 samples and surface contact angle measurement of TiO_2 films before and after dye-sensitization operation for different time periods. (a) Ex situ low temperature (90 K) ESR spectra of different P25 TiO_2 methanol-acetonitrile samples following UV irradiation (BP 365 nm) for different irradiation times (0−12 h) without RhB. (b) Ex situ low-temperature (90 K) ESR spectra of different P25 TiO_2 methanol-acetonitrile samples containing 10^{-5} M RhB following visible-light irradiation (BP 550 nm) for different irradiation times (0−12 h). (c) Surface contact angle measurements of TiO_2 film samples during continuous dye-sensitization operation (top) and UV-direct excitation as control (bottom). Prior to the measurement, the corresponding TiO_2 film was immersed in methanol (with 10^{-5} M RhB for the sensitized case) and irradiated with either visible or UV light for different times (0−12 h). The film sample was then removed and dried under an argon atmosphere. The TiO_2 film coated onto FTO (3 cm × 2.5 cm) was prepared by the hydrothermal method reported in the literature.[30]

indicate that another hidden factor involving the ET and PT on TiO_2 surface is actually responsible for the PCE failure.

To examine whether the hydrogen species corresponding to the peak at 1.292 ppm is generally formed by dye-sensitized chemical reactions, we investigated TiO_2 particle suspension solution systems with different dyes and solvents under visible light irradiation using MAS ^{1}H NMR spectroscopy. We used the most common P25 TiO_2 particles suspended in an anaerobic alcohol solution (also as a proton donor) as the typical dye-sensitizing reaction (equivalent to the open-circuit state in DSSC operation). Prior to irradiation, the P25 TiO_2 samples dried from methanol showed two peaks of MAS ^{1}H NMR, with one clear and broad peak at 3.939 ppm replacing the original H_2O and −OH groups (Figure 2a, b) and another, less obvious peak at 1.292 ppm (Figure 2c). The former was ascribed to the C−H signal of the methanol adsorbed on the TiO_2 surface, as was confirmed by control experiments using deuterium-substituted methanol-d_4 (Figure 2a). For the latter, exactly like the observed peak at 1.292 ppm in N719-DSSCs case (Figure 1a), we believe its occurrence before dye-sensitization operation resulted from the preparation and storage of TiO_2 samples exposed to light. Thus, we carefully treated our P25 TiO_2 particles in aqueous suspension with UV light for a prolonged period and then applied a heating treatment to eliminate the possibility of adsorbed organic compounds. All subsequent operations were conducted in an argon-filled glovebox in order to avoid water vapor or other volatile organics as potential proton source. Following the treatment, the peak at 1.292 ppm was no longer observed in the spectra (Figure 2c). However, in the systems sensitized by both the metal−organic complex N3 dye and the general organic dye Rhodamine B (RhB), the peak at 1.292 ppm emerged, and its intensity relative to the peak at 3.939 ppm increased with the increasing visible-light irradiation times (Figure 2d, e). As a control, the analogous peak at 1.292 ppm was not observed in the case of UV-excitation (Figure 2f) under otherwise identical conditions. This result distinguishes the difference between ET/PT reactions of the visible-light driven dye-sensitization and UV direct excitation on TiO_2 surface, and more importantly, confirms that this new proton-originated hydrogen species is distinctively generated by the dye-sensitized proton conversion on the TiO_2 surface independent of the dyes used or its occurrence during DSSC operation or in TiO_2-suspended solution. We also quantified trapped electrons of dye-sensitized TiO_2 by the Fe(III)-1, 10-phenanthroline titration method (as described in the Supporting Information, Supplementary Figure 3). According to the electron titration results, the saturated electron storage capacities for dye-sensitization accounted for ∼3% of the total Ti atoms of TiO_2 and ∼100 ± 10% of the surface Ti sites (calculated relative to a perfect anatase {101} surface).

ESR Observation of Dye-Sensitized TiO_2. In the traditional view, dye-injected electrons on TiO_2 are transferred by the reversible Ti^{4+}/Ti^{3+} redox relaxation circle acting as the electron trapping relay, identical to the case of direct TiO_2 excitation by <387 nm UV light.[15] Thus, the generation of Ti^{3+} states can be readily detected by *ex situ* electron-spin resonance (ESR) spectroscopy at low temperature (90 K). As depicted in Figure 3a, in the conventional UV direct excitation case, a strong signal at $g_{\|}$ = 1.95 was observed in the ESR spectrum of a P25 TiO_2 anaerobic suspension system (alcohol as the sacrificial reagent); this signal increased quickly in intensity with the increasing irradiation time. The signal at $g_{\|}$ = 1.95 was assigned to the Ti^{3+} state generated by Ti^{4+} reduction by the trapping of photogenerated electrons, in good agreement with previously reported results and supporting the 1e-trapped mechanism.[15] By contrast, under dye-sensitized conditions (Figure 3b), no Ti^{3+} ESR signals were observed at $g_{\|}$ = 1.95, even though the quantity of trapped electrons determined by the Fe(III)-1,10-phenanthroline spectrophotometric titration

DOI: 10.1021/jacs.6b12324
J. Am. Chem. Soc. 2017, 139, 2083−2089

(described in the Supporting Information) was nearly identical to that in the UV case (Supplementary Figure 3). Without exception, this silent ESR phenomenon was also observed when the metal−organic complex dye sensitizers (N3/N719-Ru dyes) were used and when other alcohols were used as the sacrificial reagent (Supplementary Figure 4). This silent ESR phenomenon indicates that the final form of the visible-light-driven dye-injected electrons and released protons from alcohol oxidation is not the transient stable $Ti^{3+}(-OH^{+})$ species from the reversible PCET reaction $Ti_{5c}^{4+}-OH_{surf.} + e^{-}_{cb}$ $(+ H^{+}) \leftrightarrow Ti_{4c}^{3+} + (H^{+})^{-}OH_{ad}$, which should exhibit a specific Ti^{3+} signature in ESR spectra.[15] The combined results of the new proton form (1.292 ppm ^{1}H MAS NMR) and saturated electron trapping number (nearly identical to the UV case, Supplementary Figure 3a, b) indicated that the dye-sensitized TiO_2 possesses a different reduced Ti (not Ti^{3+}) or H form on the TiO_2 surface, which is possibly a new Ti−H species rather than the traditional $Ti^{3+}O^{-}-H^{+}$ group as in the UV case. To further validate this assignment, we also directly examined the MAS−^{1}H NMR spectra of a commercial titanium hydride (TiH_2) solid powder sample (orange line in Figure 2e). The chemical shift of the main peak of the spectrum of the TiH_2 sample was identical to that of the newly formed H species of the dye-sensitized samples, 1.292 ppm. In addition, the characterization of the pure TiH_2 sample by ESR (Supplementary Figure 5) revealed the absence of the diagnostic peak of the Ti^{3+} state ($g_{\|}$ = 1.95), consistent with our expectations.

In situ Tracing the Formation of Ti−H Surface Species by Isotopic Labeled ATR-FTIR Spectroscopy. We further used isotopic *H*/*D* and $^{48}Ti/^{49}Ti$-labeled alcohol and TiO_2 for in situ tracing of the possible Ti−H species formed on the TiO_2 surface by attenuated total reflection Fourier transform infrared spectroscopy (ATR-FTIR). When RhB/TiO_2/methanol-d_0 was used as the ATR-FTIR sample and irradiated in situ with a 550 nm LED lamp, peaks at 2835 and 2944 cm^{-1} and a very weak peak at 2981 cm^{-1} emerged from the background and increased in intensity with increasing irradiation time (Figure 4a). These three peaks were very similar to those in the spectrum of the TiH_2 solid sample (top of Figure 4a) and were assigned to the symmetric stretching vibration and antisymmetric stretching vibration of the Ti−H bond (given the coexistence of symmetric and antisymmetric stretching vibrations, Ti−H surface species should be in the $\equiv Ti-H_2$ nonlinear configuration). Identical features were observed when RhB was replaced with other dyes such as the N3 dye, when the alcohol was replaced with other proton/electron donors such as isopropanol or ethanol, or when the P25 TiO_2 film was replaced with a commercial anatase TiO_2 film (Supplementary Figure 6). When we replaced methanol-d_0 with methanol-d_4 under otherwise identical conditions (Figure 4b), three newly generated diagnostic peaks emerged at 2070 cm^{-1}, 2214 cm^{-1}, and 2245 cm^{-1} in terms of the theoretical H/D replacement effect. This result is also consistent with the ATR-FTIR data for the synthesized TiD_2 sample (XRD spectra, see Supplementary Figure 5c), in which Ti-D signals were observed at 2072 and 2225 cm^{-1} (the broad signal at 2225 cm^{-1} was likely the overlying peak of 2214 and 2245 cm^{-1}, top of Figure 4b). To further identify the species related to both protons and surface Ti atoms of TiO_2, we replaced the P25 TiO_2 film with an isotopically labeled TiO_2-^{49}Ti film (^{49}Ti isotopic abundance: approximately 93.3%, see Supplementary Figure 7). The symmetric stretching and antisymmetric stretching vibrations of the Ti−H bond both shifted toward lower wavenumbers (by approximately 10 cm^{-1}) upon the replacement of $^{48}Ti-H$ with $^{49}Ti-H$ (Figure 4c). We simultaneously replaced both methanol-d_0 and the TiO_2 film with methanol-d_4 and a TiO_2-^{49}Ti film. The signals for ^{49}Ti-D (Figure 4d) were observed with a shift of a few wavenumbers from those of ^{48}Ti-

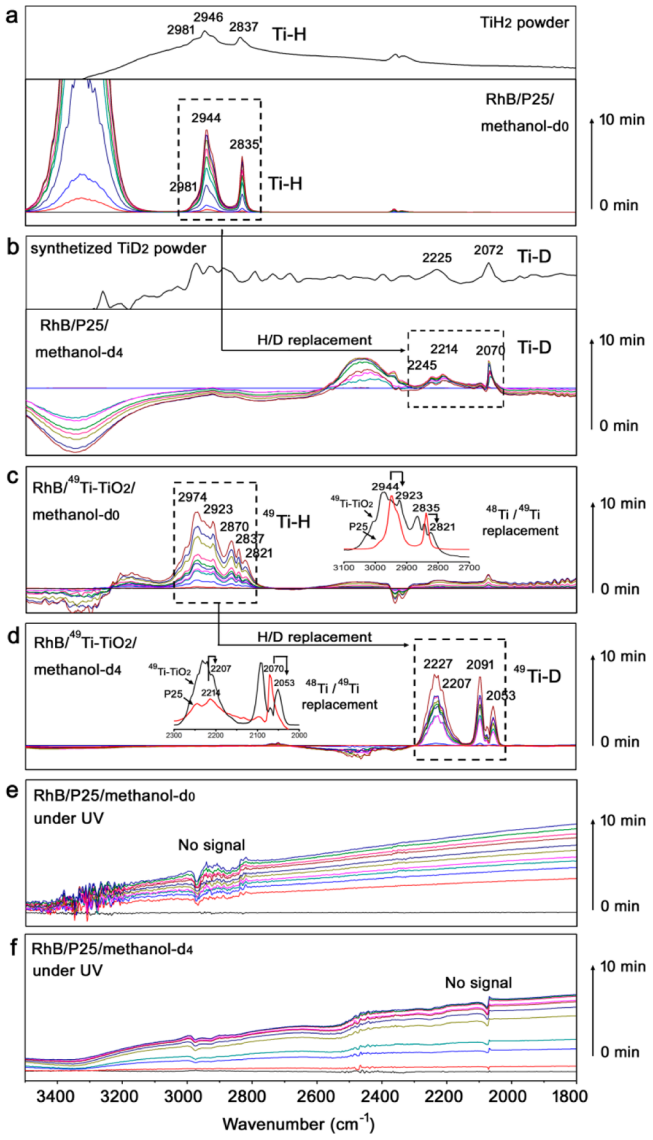

Figure 4. Isotopically labeled ATR-FTIR spectra of photocharged TiO_2 films. (a) ATR-FTIR spectra collected from a TiO_2 film immersed in 10^{-5} M RhB methanol solution under in situ irradiation by a constant 550 nm LED lamp; the top inset is the ATR-FTIR spectrum of commercial TiH_2 dispersed on a TiO_2 film as a control. (b) Identical to (a) except that methanol was replaced with methanol-d_4; the top inset shows the result for a deuterium-labeled TiD_2 sample (synthesized by heating Ti powder in D_2/Ar (5%) gas) dispersed on a TiO_2 film as the control. (c) Identical to (a), except that TiO_2 was replaced with a ^{49}Ti-labeled TiO_2 film; the inset is the magnified spectrum of ^{49}Ti-labeled and unlabeled TiO_2 between 2700 and 3100 cm^{-1}, illustrating the $^{48/49}Ti$ isotopic replacement effect. (d) Identical to (b), except that TiO_2 was replaced with a ^{49}Ti-labeled TiO_2 film; the inset is the magnified spectrum of ^{49}Ti-labeled and unlabeled TiO_2 between 2300 and 2000 cm^{-1} to illustrate the $^{48/49}Ti$ isotopic replacement effect. (e) ATR-FTIR spectra collected for a TiO_2 film immersed in methanol with 10^{-5} M RhB dye under in situ irradiation by a constant 365 nm UV-light LED lamp. (f) Identical to (e), except that methanol was replaced with methanol-d_4.

DOI: 10.1021/jacs.6b12324
J. Am. Chem. Soc. 2017, 139, 2083−2089

D, with a clear H/D replacement effect on the ^{49}Ti−H signals. Together with the H/D replacement experiments, the shifts of the ATR-FTIR peaks of ^{49}Ti−H/D, compared to those of the unlabeled ^{48}Ti−H/D, provide direct evidence for the formation of Ti−H surface species during visible-light-driven dye sensitization in the dye/alcohol/TiO_2 system. As a control, in an otherwise identical system under UV irradiation by a 365 nm LED lamp (Figures 4e, f), obvious baseline upshifts (in the broad range from 3400 to 1000 cm^{-1}) were observed in both the methanol-d_0 and -d_4 cases instead of the Ti−H/Ti-D diagnostic signal peaks and were confidently assigned as the Ti^{3+} species generated by electron trapping,[24,25] because no obvious H/D replacement effect was observed as reported previously.[26]

The Causes of PCE Failure of Dye-Sensitized Devices by Ti−H Formation. The formation of such Ti−H surface species covering the surface of the TiO_2 film or particles will significantly reduce the efficiency of the dye-sensitized systems through two types of effects: the dramatic change in the inherent hydrophilic nature of the TiO_2 surface and blocking of the interfacial ET through the TiO_2 from the surface into the bulk. To this end, we performed surface contact angle measurements on TiO_2 films before and after dye-sensitization reactions (Figure 3c and Supplementary Figure 8e, f). The surface contact angle (CA) of the film increased from 36 ± 1° to 70 ± 2° after 12 h of visible-light irradiation. The decline of hydrophilicity caused by the dye-sensitization operation differed in striking ways from the pattern induced by UV-light irradiation, in which the CA decreased from 54 ± 2° to 22 ± 2° upon UV light irradiation, consistent with the well-reported photoinduced superhydrophilic surface of TiO_2[27,28] and with the result observed even for direct visible-light excitation on N-doped TiO_2.[29] This change in the hydrophilic nature of the TiO_2 film surface was also observed in TiO_2 particle-suspended systems: the TiO_2 particles settled very fast in methanol or slower in acetonitrile after visible-light irradiation, whereas the opposite sedimentation tendency was observed after UV-excited electron trapping (Supplementary Figure 8a, b). This change in surface polarity (without an obvious change in the size of the particles, as indicated by TEM observations, Supplementary Figure 8c, d) significantly affects the relative adsorption of polar group-anchored dyes, reagents, or electrolytes, such as the I^-/I_3^- ion pairs, and therefore affects the ET behaviors of whole dye-sensitized system. To demonstrate this effect, we traced the adsorption of I^- onto the TiO_2 films and the adsorption of benzoic acid (BA) (to represent carboxyl-anchored reagents) onto the TiO_2 particles in suspended systems as a function of the accumulated Ti−H formation. Under our experimental conditions, an obvious decrease in the adsorption capacities of I^- on the TiO_2 films (by ca. 36%) was observed with the accumulation of the Ti−H surface species in the N3-sensitized case (Supplementary Figure 9a), whereas the decrease in BA adsorption capacity on the TiO_2 particles in the suspended system (by ca. 61%) was also observed in the RhB case (Supplementary Figure 9b).

Second, a TiH_x-covered layer is an ionic conductor that achieves conduction through the transport of H^- and H^+ ions, whereas the pristine TiO_2 crystal is an n-type electrical semiconductor that transports electrons between neighboring Ti^{3+}/Ti^{4+} atoms in DSSCs. Such an accumulation of Ti−H species on the TiO_2 surface will substantially block interfacial charge transfer on TiO_2 from the surface into the bulk phase and subsequently to the external circuit. Indeed, we observed a very rapid increase in the equivalent series resistance (*Rs*) of N719-DSSCs during continuous operation under 100 mW/cm^2 AM1.5 irradiation (Supplementary Figure 10). With the addition of methanol as an extra proton donor into the electrolyte, the *Rs* value increased 3 times faster than that in the standard cells, coinciding with the rapidly decreased *Jsc* and PCE values of DSSCs and the surface accumulation of the Ti−H species (Figure 1c, d). After 25 h of operation, the normal and methanol-added cells retained only 17% and 9% of their conductivity, respectively. The electrochemical impedance spectroscopy (EIS) measurement also confirms this phenomenon (Supplementary Figure 11) as the interfacial charge transfer resistance (R_{ct}) of the TiO_2 film almost doubled after 20 h dye-sensitization operation.

CONCLUSION

The formation of Ti−H species on the TiO_2 surface is a previously unrecognized event that significantly affects the PCE of TiO_2-based dye-sensitization applications, including DSSCs, photocatalysis, and even TiO_2-based perovskite solar cells, by blocking interfacial ET and reducing the hydrophilic nature of TiO_2 surface. For TiO_2-based dye-sensitized devices or even perovskite cells, the failure of PCE is completely controlled by the extent of the nearly inevitable Ti−H species coverage. Once Ti−H species cover a certain area on the TiO_2 photoanode surface, the PCE of the device is dramatically decreased and even completely lost without the loss of dyes and electrolyte. Our present study is the first to identify the unrevealed cause that is responsible for the PCE failure of TiO_2-based dye-sensitized devices. To overcome this defect, new technologies such as avoiding the use of reagents containing protons or potential proton sources in the assembly of DSSCs or the design of other dye-sensitized systems to prevent or restrain the formation of Ti−H surface species to the greatest extent possible are needed.

ASSOCIATED CONTENT

Supporting Information

The Supporting Information is available free of charge on the ACS Publications website at DOI: 10.1021/jacs.6b12324.

Supplementary methods (including DSSCs and PSCs fabrication, Fe(III)-1,10-phenanthroline spectrometric titration, LATOF-MS and EIS measurements), experimental apparatus, and figures (including all controlled experiments and supplementary data) (PDF)

AUTHOR INFORMATION

Corresponding Authors

*whma@iccas.ac.cn

*jczhao@iccas.ac.cn

ORCID

Shenggui He: 0000-0002-9919-6909

Chuncheng Chen: 0000-0003-4034-8063

Wanhong Ma: 0000-0001-9117-9090

Notes

The authors declare no competing financial interest.

ACKNOWLEDGMENTS

This work was supported by the 973 project (No. 2013CB632405), NSFC (Nos. 21590811, 21521062, 21377134, 21525729), the "Strategic Priority Research

DOI: 10.1021/jacs.6b12324
J. Am. Chem. Soc. 2017, 139, 2083−2089

Program" of the Chinese Academy of Sciences (No. XDA09030200), and the Postgraduate Innovation Project of Jiangsu Province (No. KYLX_1045).

REFERENCES

(1) O'Regan, B.; Gratzel, M. *Nature* **1991**, *353*, 737−740.
(2) Hagfeldt, A.; Boschloo, G.; Sun, L.; Kloo, L.; Pettersson, H. *Chem. Rev.* **2010**, *110*, 6595−6663.
(3) Yella, A.; Lee, H. W.; Tsao, H. N.; Yi, C.; Chandiran, A. K.; Nazeeruddin, M. K.; Diau, E. W.; Yeh, C. Y.; Zakeeruddin, S. M.; Grätzel, M. *Science* **2011**, *334*, 629−634.
(4) Willkomm, J.; Orchard, K. L.; Reynal, A.; Pastor, E.; Durrant, J. R.; Reisner, E. *Chem. Soc. Rev.* **2016**, *45*, 9−23.
(5) Youngblood, W. J.; Lee, S. H.; Kobayashi, Y.; HernandezPagan, E. A.; Hoertz, P. G.; Moore, T. A.; Moore, A. L.; Gust, D.; Mallouk, T. E. *J. Am. Chem. Soc.* **2009**, *131*, 926−927.
(6) Xiao, F.; Wang, M.; Wang, F.; Xia, X. *Small* **2014**, *10*, 706−716.
(7) Zhang, M.; Chen, C.; Ma, W.; Zhao, J. *Angew. Chem., Int. Ed.* **2008**, *47*, 9730−9733.
(8) Li, Q.; Che, Y.; Ji, H.; Chen, C.; Zhu, H.; Ma, W.; Zhao, J. *Phys. Chem. Chem. Phys.* **2014**, *16*, 6550−6554.
(9) Lee, S. H.; Park, Y.; Wee, K. R.; Son, H. J.; Cho, D. W.; Pac, C.; Choi, W.; Kang, S. O. *Org. Lett.* **2010**, *12*, 460−463.
(10) Zhang, M.; Chen, C.; Ma, W.; Zhao, J. *Angew. Chem., Int. Ed.* **2008**, *47*, 9730−9733.
(11) Saliba, M.; Matsui, T.; Seo, J.-Y.; Domanski, K.; Correa-Baena, J. P.; Nazeeruddin, M. K.; Zakeeruddin, S. M.; Tress, W.; Abate, A.; Hagfeldt, A.; Grätzel, M. *Energy Environ. Sci.* **2016**, *9*, 1989−1997.
(12) Onda, K.; Li, B.; Zhao, J.; Jordan, K. D.; Yang, J.; Petek, H. *Science* **2005**, *308*, 1154−1158.
(13) Savory, D.; McQuillan, A. *J. Phys. Chem. C* **2013**, *117*, 23645−23656.
(14) (a) Xu, C.; Yang, W.; Guo, Q.; Dai, D.; Chen, M.; Yang, X. *J. Am. Chem. Soc.* **2014**, *136*, 602−605. (b) Pichat, P. *New J. Chem.* **1987**, *11*, 135−140.
(15) (a) Schrauben, J. N.; Hayoun, R.; Valdez, C. N.; Braten, M.; Fridley, L.; Mayer, J. M. *Science* **2012**, *336*, 1298−1301. (b) Dyrek, C.; Schindler, R. *Z. Naturforsch., A: Phys. Sci.* **1977**, *32*, 501−504.
(16) Halverson, A. F.; Zhu, K.; Erslev, P. T.; Kim, J. Y.; Neale, N. R.; Frank, A. J. *Nano Lett.* **2012**, *12*, 2112−2116.
(17) (a) Swierk, J.; McCool, N.; Saunders, T.; Barber, G.; Mallouk, T. *J. Am. Chem. Soc.* **2014**, *136*, 10974−10982. (b) McCool, N. S.; Swierk, J. R.; Nemes, C. T.; Saunders, T. P.; Schmuttenmaer, C. A.; Mallouk, T. E. *ACS Appl. Mater. Interfaces* **2016**, *8*, 16727−16735.
(18) Rittmann-Frank, M. H.; Milne, C. J.; Rittmann, J.; Reinhard, M.; Penfold, T. J.; Chergui, M. *Angew. Chem., Int. Ed.* **2014**, *53*, 5858−5862.
(19) Zhang, J.; Steigerwald, M.; Brus, L.; Friesner, R. A. *Nano Lett.* **2014**, *14*, 1785−1789.
(20) Pathak, S. K.; Abate, A.; Leijtens, T.; Hollman, D. J.; Teuscher, J.; Pazos, L.; Docampo, P.; Steiner, U.; Snaith, H. J. *Adv. Energy Mater.* **2014**, *4*, 1301667.
(21) Berginc, M.; Topic, M.; Opara Krašovec, U. *Phys. Chem. Chem. Phys.* **2014**, *16*, 12940−12948.
(22) Ruud, H. M. *J. Chem. Soc., Faraday Trans.* **1996**, *92*, 2791−2798.
(23) Zhang, H.; Yu, H.; Zheng, A.; Li, S.; Shen, W.; Deng, F. *Environ. Sci. Technol.* **2008**, *42*, 5316−5321.
(24) Warren, D.; McQuillan, A. *J. Phys. Chem. B* **2004**, *108*, 19373−19379.
(25) Szczepankiewicz, S.; Moss, J.; Hoffmann, M. *J. Phys. Chem. B* **2002**, *106*, 2922−2927.
(26) Panayotov, D. A.; Yates, J. T. *Chem. Phys. Lett.* **2007**, *436*, 204−208.
(27) Lee, K.; Kim, Q.; An, S.; An, J.; Kim, J.; Kim, B.; Jhe, W. *Proc. Natl. Acad. Sci. U. S. A.* **2014**, *111*, 5784−5789.
(28) Wang, R.; Hashimoto, K.; Fujishima, A.; Chikuni, M.; Kojima, R.; Kitamura, A.; Shimohigoshi, M.; Watanabe, T. *Nature* **1997**, *388*, 431−432.
(29) Asahi, R.; Morikawa, T.; Ohwaki, T.; Aoki, K.; Taga, Y. *Science* **2001**, *293*, 269−271.
(30) Mali, S. S.; Betty, C. A.; Bhosale, P. N.; Patil, P. S.; Hong, C. K. *Sci. Rep.* **2014**, *4*, 5451.
(31) Almeida, A.; Moulijn, J. A.; Mul, G. *J. Phys. Chem. C* **2008**, *112* (5), 1552−1561.
(32) Chang, W.; Sun, C.; Pang, X.; Sheng, H.; Li, Y.; Ji, H.; Song, W.; Chen, C.; Ma, W.; Zhao, J. *Angew. Chem., Int. Ed.* **2015**, *54* (7), 2052−2056.

DOI: 10.1021/jacs.6b12324
J. Am. Chem. Soc. 2017, 139, 2083−2089